

# A Way to 3D Numerical Relativity — Coalescing Binary Neutron Stars —

Takashi NAKAMURA

Yukawa Institute for Theoretical Physics  
Kyoto University, Kyoto 606-01, Japan

Ken-ich Oohara

Department of Physics, Niigata University  
Niigata, 950-2181, Japan

## 1 Introduction

Long baseline interferometers to detect gravitational waves such as TAMA300 [1], GEO600 [2], VIRGO [3], LIGO [4] will be in operation by the end of this century or the beginning of the 21st century. One of the most important sources of gravitational waves for such detectors are coalescing binary neutron stars. PSR1913+16 is the first binary neutron stars found by Hulse and Taylor. The existence of the gravitational waves is confirmed by analyzing the arrival time of radio pulses from PSR1913+16. At present there are three systems like PSR1913+16 for which coalescing time due to the emission of gravitational waves is less than the age of the universe. From these observed systems the event rate of the coalescing binary neutron stars is estimated as  $10^{-6} \sim 2 \times 10^{-5}$  events  $\text{yr}^{-1} \text{ galaxy}^{-1}$  [5, 6, 7]. From the formation theory of binary neutron stars, the event rate is estimated as  $2 \times 10^{-5} \sim 3 \times 10^{-4}$  events  $\text{yr}^{-1} \text{ galaxy}^{-1}$  [8, 9, 10]. If the event rate is  $\sim 2 \times 10^{-5}$ , two different methods yield the agreement. Since the number density of galaxies is  $\sim 10^{-2}/\text{Mpc}^3$ , we may expect several coalescing events/year within 200Mpc ( $\sim 2 \times 10^{-7}$  events / $\text{Mpc}^3$ ). The coalescing binary neutron stars is a possible central engine of cosmological gamma ray bursts. Coalescing binary neutron stars is also a possible site of r-process element production.

The eccentricity  $e$  and the semimajor axis  $a$  of binary neutron stars decrease due to the emission of gravitational waves, and these quantities are related with each other as

$$e = e_0 \left( \frac{a}{a_0} \right)^{\frac{19}{12}} \quad (1)$$

where  $e_0$  and  $a_0$  are the initial eccentricity and the semimajor axis, respectively [11, 12]. If  $a_0 \sim R_\odot$  like PSR1913+16,  $e \sim 10^{-6}$  for  $a \sim 500\text{km}$  so that the orbit is almost circular. The merging time  $t_{\text{mrg}}$  due to the emission of the gravitational waves is given by

$$t_{\text{mrg}} = 3 \min \left( \frac{m_1}{1.4M_\odot} \right)^{-1} \left( \frac{m_2}{1.4M_\odot} \right)^{-1} \left( \frac{m_1 + m_2}{2.8M_\odot} \right)^{-1} \left( \frac{a}{470\text{km}} \right)^4, \quad (2)$$

where  $m_1$  and  $m_2$  are each mass of neutron stars. The frequency of the gravitational waves  $\nu_{\text{GW}}$  is given by

$$\nu_{\text{GW}} = 19\text{Hz} \left( \frac{m_1 + m_2}{2.8M_\odot} \right)^{\frac{1}{2}} \left( \frac{a}{470\text{km}} \right)^{-\frac{3}{2}} \quad (3)$$

This is just the frequency range ( $\nu_{\text{GW}} = 10\text{Hz} \sim 1\text{kHz}$ ) of long baseline interferometers to detect gravitational waves such as TAMA300, GEO600, VIRGO, LIGO. The number of rotation before the final merge is given by

$$N = 2635 \left( \frac{m_1}{1.4M_\odot} \right)^{-1} \left( \frac{m_2}{1.4M_\odot} \right)^{-1} \left( \frac{m_1 + m_2}{2.8M_\odot} \right)^{-\frac{1}{2}} \left( \frac{a}{470\text{km}} \right)^{\frac{5}{2}} \quad (4)$$

The merging phase of coalescing binary neutron stars is divided into two stages; 1) The last three minutes [13] and 2) The last three milliseconds. In the first stage  $a$  is much larger than the neutron star radius  $R_{\text{NS}}$  and the rotation velocity of the binary  $v_r$  is  $\sim 0.05c$  so that each neutron star can be considered as a point particle. The post-Newtonian expansion will converge in the first stage. However the quite accurate theoretical calculations of the wave form are needed since only the uncertainty of  $1/2635$  in the theoretical prediction of the energy loss will cause one rotation ambiguity at last. If the accurate theoretical template is obtained [14], by making a cross correlation with the observational data we may determine each mass, spin, inclination and the distance of binary neutron stars [15].

In the second stage  $a$  is comparable to  $R_{\text{NS}}$  and the gravity is so strong that the post-Newtonian expansion is not a good approximation and the finite size effect of neutron stars is important. In the final collision phase, the general relativistic hydrodynamics are also important. Only 3D numerical relativity can study this important final merging phase related to gravitational waves, gamma ray burst and production of r-process elements.

## 2 Newtonian Simulations

To clarify the phenomena in the last three milliseconds many numerical simulations have been done so far. They are classified into several categories.

### A) Newtonian hydrodynamics without radiation reaction

In this category, using the Newtonian hydrodynamics, equilibria and stability of the binary neutron stars are studied for various initial parameters and equation of states [16, 17, 18, 19, 20, 21, 22].

### B) A) + simple radiation reaction up to contact of neutron stars

In this category, radiation reaction is included so that the binary spirals in due to the emission of the gravitational waves. However after the contact the radiation reaction is switched off [23, 24, 25].

### C) A) + radiation reaction

In this category the radiation reaction is fully taken into account even after the contact. However the computation is time consuming because to estimate the radiation reaction potential two more Poisson equations other than the Poisson equation for the Newtonian gravitational potential should be solved [17, 26, 27, 28, 29, 30, 31, 33].

In Fig.1 we show an typical example of such a simulation [26]. In this case each mass of the binary is the same. We start the simulation from the equilibrium obtained in category **A)**. Due to the loss of the angular momentum by gravitational waves the merging starts spontaneously. As merging proceeds, two arm spiral extends outward. The spiral arms become tightly bound later and becomes a disk. The final result is an almost axially symmetric central object and a disk around it. In Fig.1 the thick circle shows the Schwarzschild radius of the total mass. Although it is not possible to say the formation of a black hole in Newtonian simulations, we expect that the central object is a black hole. So the final destiny may be a black hole and a disk. This behavior is seen also in many other simulations in category **B)** and **C)**. In Fig.2 we show a typical wave pattern of the gravitational waves.

In Fig.3, a simulation for different mass case is shown[27]. In this case the lighter neutron star (left in Fig.3-a) is tidally disrupted by the heavier neutron star. We see only one arm. However the final object is more or less similar to the equal mass case, that is, a black hole and a disk. This final object may be relevant to the central engine of gamma ray burst. Ruffert will discuss in this volume on the coalescing binary neutron stars and gamma ray bursts using their simulations including the emission of neutrinos[30, 31].

### D) A)+1PN effect of Post Newtonian Hydrodynamics and Radiation Reaction

Since neutron stars are general relativistic compact objects, the Newtonian hydrodynamics is zeroth approximation to the problem. One possible refinement is to include 1PN force [i.e.  $O((v/c)^2)$  effect of the general relativistic gravity after the Newtonian gravity]. Oohara and Nakamura performed

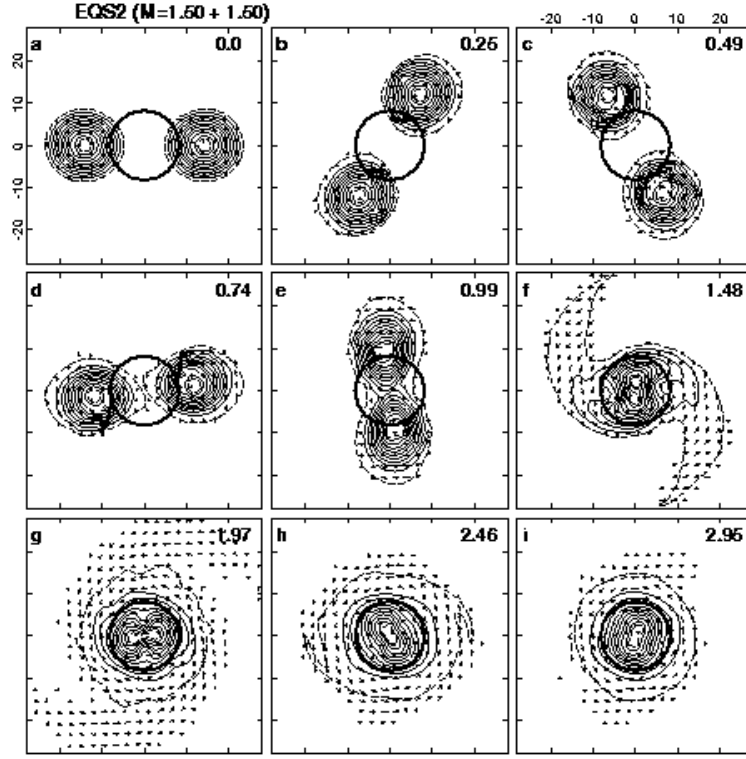


Figure 1: Density and velocity on the  $x$ - $y$  plane for EQSP2. The time in units of milliseconds is shown. Arrows indicate the velocity vectors of the matter. A fat line shows a circle of radius  $2GM_t/c^2$ .

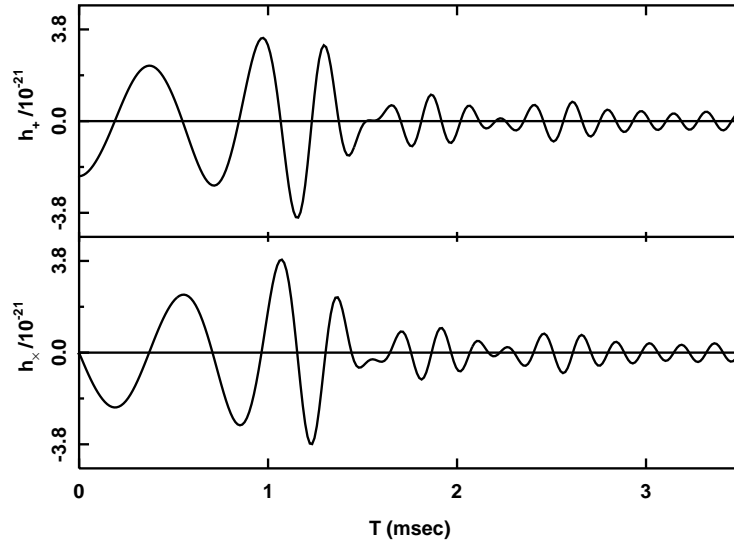


Figure 2: Wave forms of  $h_+$  and  $h_x$  observed on the  $z$ -axis at 10Mpc for EQSP2.

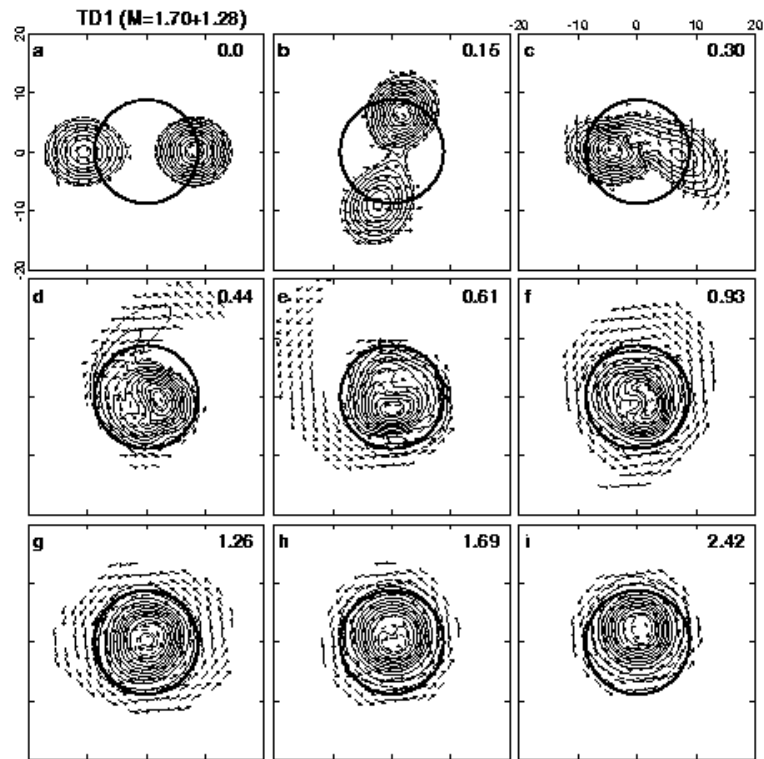


Figure 3: Density and velocity on the  $x$ - $y$  plane for TD1.

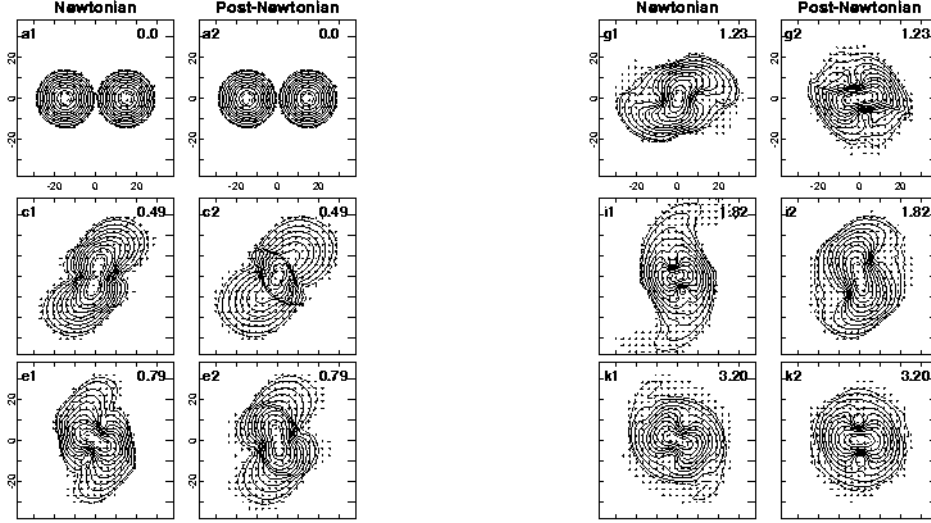


Figure 4: Density and velocity on the  $x$ - $y$  plane. The left and right figures are for the Newtonian (N) and post-Newtonian (PN) calculations, respectively. Notations are the same as for Fig.1.

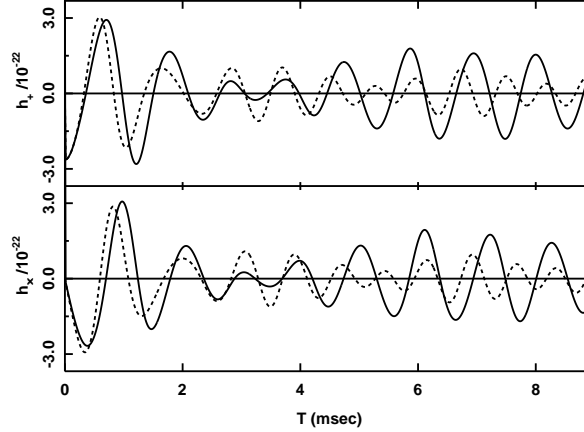


Figure 5: Wave forms of  $h_+$  and  $h_\times$  observed on the  $z$ -axis at 10Mpc. The solid and dashed lines are for PN and N, respectively.

such a simulation [32]. They first include 1PN force to the simulation in Fig.1 and found that the 1PN effect is too strong. They decrease the mass of the neutron star to  $0.62M_\odot$  from  $1.5M_\odot$  keeping the radius of the neutron the same so that the gravity becomes weaker. To see the difference between Newtonian and 1PN cases, in Fig.4 two simulations from the same initial data are shown [32]. We clearly found that they are different even in this rather weak gravity case. In Fig.5 the wave forms are shown. The solid line (1PN) and the dashed line (Newton) are different. Due to the strong gravity effect of 1PN force, the strong shock in the central is formed and the coalescence is delayed. If the higher post Newtonian effects (2PN,...) are included, different results may be obtained. This suggests that fully general relativistic simulations are needed. This suggests also that all the results of coalescing binary neutron stars based on Newtonian hydrodynamics or Post-Newtonian hydrodynamics need to be viewed with caution.

There is another point to be considered. Suppose the point particle limit of each neutron star. In the Newtonian gravity there exists a circular orbit for any small separation  $a$ . However in general

relativity a stable circular orbit does not exist for  $a < r_{\text{ISCO}}$  where ISCO stands for Innermost Stable Circular Orbit. For a test particle motion in the Schwarzschild black hole  $r_{\text{ISCO}} = 6GM/c^2$  where  $M$  is the mass of black hole. For equal mass point mass binary  $r_{\text{ISCO}}$  is estimated as  $\sim 14Gm/c^2$  where  $m$  is each mass of the binary [34]. Since the radius of the neutron star is  $\sim 5Gm/c^2$ , when two neutron stars contact, the separation  $a$  is  $\sim 10Gm/c^2$ , which is comparable to  $r_{\text{ISCO}}$  in the point particle limit. Therefore in the last three milliseconds the general relativity is also important in the orbital motion. Recently ISCO for binary neutron stars including the effect of general relativity and the finite size of the neutron stars has been extensively studied. Shibata discusses ISCO problem in this volume.

### 3 General Relativistic Simulations

For full general relativistic 3D simulations of coalescing binary neutron stars, we need ISCO of binary neutron stars as initial data. However at present such initial data are not available. We therefore discuss the development of 3D general relativistic code and test simulations. We present only the summary of the basic equations. For details of formalisms, basic equations and numerical methods please refer [35].

#### 3.1 Basic Equations

##### 3.1.1 Initial Value Equations

We adopt the (3+1)-formalism of the Einstein equation. Then the line element is written as

$$ds^2 = -\alpha^2 dt^2 + \gamma_{ij}(dx^i + \beta^i dt)(dx^j + \beta^j dt), \quad (5)$$

where  $\alpha$ ,  $\beta^i$  and  $\gamma_{ij}$  are the lapse function, the shift vector and the metric of 3-space, respectively. The lapse and shift represent the coordinate degree of freedom and its choice is essential for numerical simulations.  $\gamma_{ij}$  is dynamical variable including gravitational waves.

We assume the perfect fluid. The energy momentum tensor is given by

$$T_{\mu\nu} = (\rho + \rho\varepsilon + p)u_\mu u_\nu + pg_{\mu\nu}, \quad (6)$$

where  $\rho$ ,  $\varepsilon$  and  $p$  are the proper mass density, the specific internal energy and the pressure, respectively, and  $u_\mu$  is the four-velocity of the fluid. We define  $\rho_H \equiv n^\mu n^\nu T_{\mu\nu}$ ,  $J_i \equiv -h_i^\mu n^\nu T_{\mu\nu}$  and  $S_{ij} \equiv h_i^\mu h_j^\nu T_{\mu\nu}$  where  $n_\mu$  is the unit normal to the  $t=\text{constant}$  hypersurface and  $h_{\mu\nu} = g_{\mu\nu} + n_\mu n_\nu$  is the projection tensor to the hypersurface.

The initial data should satisfy the Hamiltonian and momentum constraint equations given by

$$R + K^2 - K_{ij}K^{ij} = 16\pi\rho_H, \quad (7)$$

$$D_j (K^j_i - \delta^j_i K) = 8\pi J_i, \quad (8)$$

where  $R$  is the 3-dimensional Ricci scalar curvature,  $K_{ij}$  is the extrinsic curvature and  $D_i$  denotes the covariant derivative with respect to  $\gamma_{ij}$ .

##### 3.1.2 Relativistic Hydrodynamics

In order to obtain equations similar to the Newtonian hydrodynamics equations, we define  $\rho_N = \sqrt{\gamma}\alpha u^0 \rho$  and  $u_i^N = J_i/\alpha u^0 \rho$  where  $\gamma = \det(\gamma_{ij})$ . Then the equation for the conservation of baryon number is expressed as

$$\partial_t \rho_N + \partial_\ell (\rho_N V^\ell) = 0, \quad (9)$$

where  $V^\ell = u^\ell/u^0$ . The equation for momentum is

$$\begin{aligned} \partial_t (\rho_N u_i^N) + \partial_\ell (\rho_N u_i^N V^\ell) = & -\sqrt{\gamma}\alpha \partial_i p - \sqrt{\gamma}(p + \rho_H) \partial_i \alpha \\ & + \frac{\sqrt{\gamma}\alpha J^k J^\ell}{2(p + \rho_H)} \partial_i \gamma_{k\ell} + \sqrt{\gamma} J_\ell \partial_i \beta^\ell. \end{aligned} \quad (10)$$

The equation for internal energy becomes

$$\partial_t(\rho_N \varepsilon) + \partial_\ell(\rho_N \varepsilon V^\ell) = -p \partial_\nu(\sqrt{\gamma} \alpha u^\nu). \quad (11)$$

To complete hydrodynamics equations, we need an equation of state,  $p = p(\varepsilon, \rho)$

### 3.1.3 Time Evolution of the Metric Tensor

The evolution equation for the extrinsic curvature which is essentially the time derivative of  $\gamma_{ij}$  is given by

$$\partial_t K_{ij} = \alpha \{ R_{ij} - 8\pi [S_{ij} + \frac{1}{2} \gamma_{ij} (\rho_H - S^\ell_\ell)] \} - D_i D_j \alpha \quad (12)$$

$$+ \alpha (K K_{ij} - 2K_{i\ell} K^\ell_j), \quad (13)$$

$$+ K_{mi} \partial_j \beta^m + K_{mj} \partial_i \beta^m - K_{ij} \partial_m \beta^m, \quad (14)$$

where  $R_{ij}$  is the 3-dimensional Ricci tensor.

Now we define the conformal factor  $\phi$  as  $\phi \equiv (\det[\gamma_{ij}])^{1/12}$  and  $\tilde{\gamma}_{ij}$  as  $\tilde{\gamma}_{ij} = \gamma_{ij}/\phi^4$ . The conformal factor  $\phi$  is determined by

$$\tilde{\Delta} \phi = -\frac{\phi^5}{8} (16\pi \rho_H + K_{ij} K^{ij} - K^2 - \phi^{-4} \tilde{R}), \quad (15)$$

where  $\tilde{\Delta}$  and  $\tilde{R}$  is the Laplacian and the scalar curvature with respect to  $\tilde{\gamma}_{ij}$ , respectively. The time evolution of  $\tilde{\gamma}_{ij}$  is given by

$$\begin{aligned} \partial_t \tilde{\gamma}_{ij} &= -2\alpha \left( \tilde{K}_{ij} - \frac{1}{3} \tilde{\gamma}_{ij} K \right) + \tilde{D}_i \tilde{\beta}_j + \tilde{D}_j \tilde{\beta}_i - \frac{2}{3} \tilde{\gamma}_{ij} \tilde{D}_\ell \tilde{\beta}^\ell \\ &\equiv A_{ij}^T, \end{aligned} \quad (16)$$

where

$$\tilde{K}_{ij} = \phi^{-4} K_{ij}, \quad \tilde{\beta}_i = \phi^{-4} \beta_i \quad (17)$$

and  $\tilde{D}_i$  denotes the covariant derivative with respect to  $\tilde{\gamma}_{ij}$ .

### 3.1.4 Coordinate Conditions

One of the most serious technical problems in numerical relativity is the control of the space and time coordinates. Difficulties arise from (a) coordinate singularities caused by strong gravity and the dragging effect, where coordinate lines may be driven towards or away from each other, and (b) spacetime singularities which appear when a black hole is formed. We should demand coordinate conditions so that these singularities can be avoided.

#### Spatial coordinates — the shift vector $\beta^i$

We demand  $\partial_i A_{ij}^T = 0$ . Then  $A_{ij}^T$  becomes transverse-traceless. Equation (16) is reduced to the equation for the shift vector  $\beta^i$  as

$$\begin{aligned} \nabla^2 \beta^i + \frac{1}{3} \partial_i (\partial_\ell \beta^\ell) &= \\ \partial_j \left[ 2\alpha \left( \tilde{K}_{ij} - \frac{1}{3} \tilde{\gamma}_{ij} K \right) \right] & \\ - \partial_j \left[ \hat{\gamma}_{j\ell} \partial_i \beta^\ell + \hat{\gamma}_{i\ell} \partial_j \beta^\ell - \frac{2}{3} \hat{\gamma}_{ij} \partial_\ell \beta^\ell + \beta^\ell \partial_\ell \hat{\gamma}_{ij} \right], & \end{aligned} \quad (18)$$

where  $\nabla^2$  is the simple flat-space Laplacian and  $\hat{\gamma}_{ij} = \tilde{\gamma}_{ij} - \delta_{ij}$ .

We require a time slice to have the following properties: (1) In the central region, spacetime singularities should be avoided. These singularities are regions of spacetime where curvature, density and other quantities are infinite. (2) In the exterior vacuum region, the metric should be stationary except for the wave parts to catch gravitational waves numerically.

The lapse function  $\alpha$  is given by

$$\alpha = \exp \left[ -2 \left( \hat{\phi} + \frac{\hat{\phi}^3}{3} + \frac{\hat{\phi}^5}{5} \right) \right], \quad (19)$$

where  $\hat{\phi} = \phi - 1$ . In this slicing, the space outside the central matter quickly approaches the Schwarzschild metric. Since the non-wave parts decrease as  $O(r^{-4})$  for large  $r$ , we can catch gravitational waves numerically with  $O((M/r_c)^3)$  accuracy, where  $M$  is mass of the system and  $r_c$  is distance from the origin of the position where gravitational waves are evaluated.

## 4 Coalescing Binary Neutron Stars in 3D Numerical Relativity

We show our test simulations of coalescing binary neutron stars. We place two spherical neutron stars of mass  $M = 1.0M_\odot$  and radius  $r_0 = 6M$  with density distribution ( $\rho_N$ ) of  $\gamma = 2$  polytrope at  $x = 7.2M$  and  $x = -7.2M$ . We add a rigid rotation with angular velocity  $\Omega$  as well as an approaching velocity to this system such that

$$v_x^N = \begin{cases} -\Omega y - \Omega r_0 & \text{if } x > 0, \\ -\Omega y + \Omega r_0 & \text{if } x < 0, \end{cases} \quad (20)$$

$$v_y^N = \Omega x. \quad (21)$$

We adopt  $(x, y, z)$  coordinates with  $201 \times 201 \times 201$  grid size (9GB) and typical CPU time being 10 hours on VPP300(FUJITU). The details of a numerical method is shown in [35].

We performed two simulations, BI1 and BI2, with different values of  $\Omega$ . The total angular momentum divided by the square of the gravitational mass are 0.99 and 1.4 and for BI1 and BI2, respectively. Figure 6 shows the evolution of the density on the  $x$ - $y$ ,  $y$ - $z$  and  $x$ - $z$  planes of BI2. The binary starts to coalesce and rotates about 180 degree. In Fig.7 we show  $flux \equiv r^2 \dot{\gamma}_{ij}^2 / 32\pi$  which can be considered as the energy flux of the gravitational wave energy if we take appropriate averaging.  $flux$  shows an interesting feature of generation and propagation of the waves. A spiral pattern appears on the  $x$ - $y$  plane while different patterns with peaks around  $z$ -axis appear on the  $x$ - $z$  and  $y$ - $z$  planes. This can be explained by the quadrupole wave pattern. In Fig.8 we show the luminosity of the gravitational waves as a function of the retarded time  $t - r$  calculated at various  $r$ . For large  $r$  it seems that the luminosity converges, which suggests that the gravitational waves are calculated correctly in our simulations.

The total energy of the gravitational radiation as a function of the retarded time is shown in Fig.9. The total energy amounts to  $4 \times 10^{-3}M$  (0.2% of the total mass) and  $1 \times 10^{-3}M$  (0.05% of the total mass) for BI2 and BI1, respectively.

In conclusion, the present test simulations suggest future fruitful development of 3D fully general relativistic simulations of coalescing binary neutron stars.

Numerical simulations were performed by VPP300 at NAO. This work was also supported by a Grant-in-Aid for Basic Research of the Ministry of Education, Culture, and Sports No.08NP0801.

## References



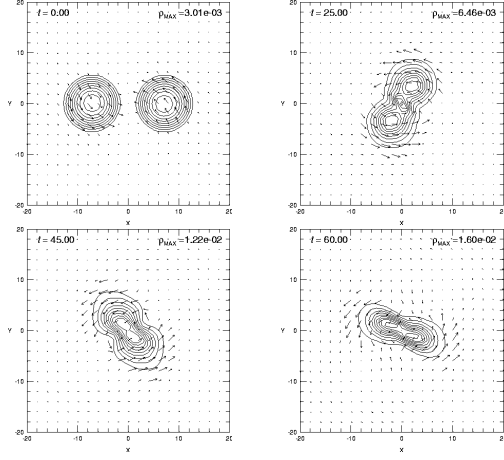


Figure 6: Mass density  $\rho_N$  on the  $x - y$  plane. Arrows indicate the velocity vector  $V^i$ . Quantities are represented in units of  $c = G = M_\odot = 1$ .

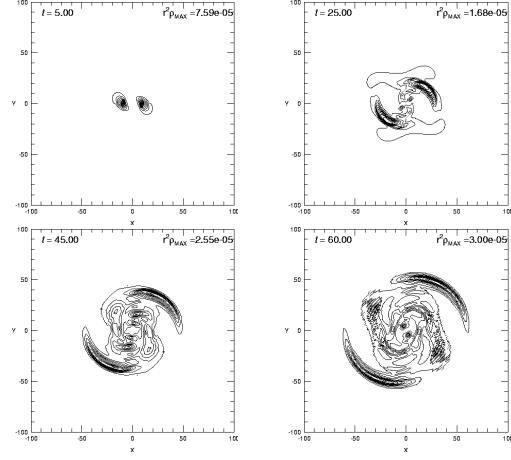


Figure 7:  $r^2 \dot{\gamma}_{ij}^2 / 32\pi$ , which is expected to represent “Energy density of the gravitational waves.”

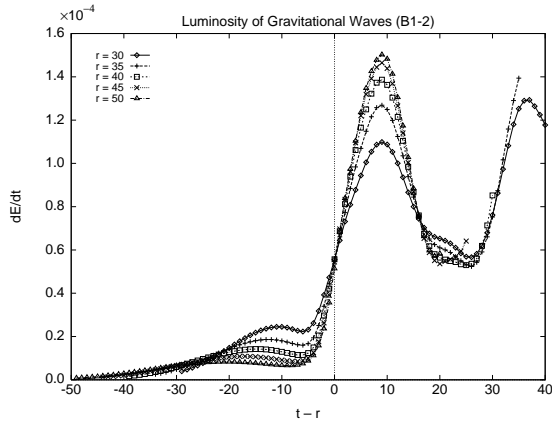


Figure 8: Luminosity of gravitational waves  $L_{\text{GW}}$  as a function of the retarded time  $t - r$  calculated at  $r = 30 \sim 50$ .

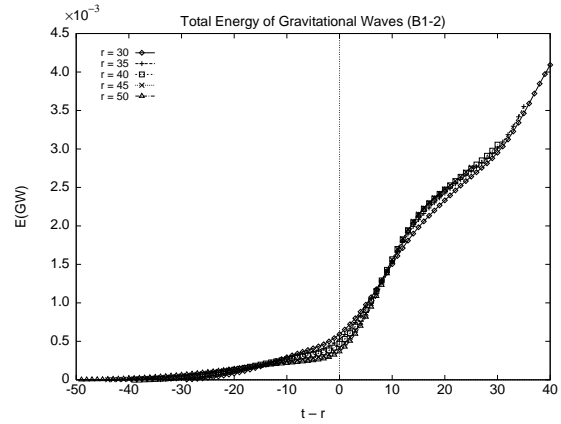


Figure 9: Energy of gravitational waves  $E_{\text{GW}}$  as a function of the retarded time  $t - r$  calculated at  $r = 30 \sim 50$ .

- [1] Tsubono, K. , in *Gravitational Wave Detection* eds, K. Tsubono, M.-K.Fujimoto and K. Kuroda, Universal Academic Press, INC.-TOKYO (November 12-14 1996 Saitama, Japan) pp.183-192
- [2] Hough, J. , in *Gravitational Wave Detection* eds, K. Tsubono, M.-K.Fujimoto and K. Kuroda, Universal Academic Press, INC.-TOKYO (November 12-14 1996 Saitama, Japan) pp.175-182
- [3] Brillet, A. , in *Gravitational Wave Detection* eds, K. Tsubono, M.-K.Fujimoto and K. Kuroda, Universal Academic Press, INC.-TOKYO (November 12-14 1996 Saitama, Japan) pp.163-174
- [4] Barish, B., in *Gravitational Wave Detection* eds, K. Tsubono, M.-K.Fujimoto and K. Kuroda, Universal Academic Press, INC.-TOKYO (November 12-14 1996 Saitama, Japan) pp.155-162
- [5] Phinney, E. S. 1991, *Astrophys. J*, 380, L17
- [6] Narayan, R. Piran, T. & Shemi, A. 1991, *Astrophys. J*, 379, L17
- [7] Van den Heuvel, E.P.J. and Lorimer, D.R. 1996, *Mon. Not. Roy. Astro. Soc.*, 283, L37
- [8] Tutukov, A.V. and Yungelson, L.R. 1994, *Mon. Not. Roy. Astro. Soc.*, 268, 871-879
- [9] Lipunov, V.M., Postnov, K.A. and Prokhorov, M.E. 1997 , *Mon. Not. Roy. Astro. Soc.*, 288, 245-259
- [10] Yungelson, L. and Zwart, S. 1998, astro-ph/9801127
- [11] Peters, P.C. & Mathews, J. 1963, *Phys. Rev.*, 131, 435
- [12] Peters, P.C. 1964, *Phys. Rev.*, 136, B1224
- [13] Cutler, C. et al. 1993, *Phys. Rev. Letters*, 70, 2984
- [14] Blanchet, L. 1996, *Phys. Rev.*, D54, 1417-1438
- [15] Cutler, C. and Flanagan, E. E. 1994, *Phys. Rev.*, 49, 2658-2697
- [16] Oohara, K. and Nakamura, T. 1989, *Prog. Theor. Phys.* 82, 535
- [17] Nakamura, T. and Oohara, K. 1989, *Prog. Theor. Phys.* 82 , 1066
- [18] Rasio, F. A. and Shapiro, S.L. 1992, *Astrophys. J*, 401, 226-245
- [19] Centrella, J.M. and McMillan, S.L.W. 1993 , *Astrophys. J*, 416, 719-732
- [20] Rasio, F. A. and Shapiro, S.L. 1994, *Astrophys. J*, 432, 242-261
- [21] Houser, J.L., Centrella, J.M. and Smith, S.G. 1989, *Phys. Rev. Letters* 72, 1314-1317
- [22] New, K.C.B., and Tohline, J.E. 1997 , *Astrophys. J*, 490, 311-327
- [23] Davies, M.B., Benz, W., Piran, T., and Thielemann F. K., 1994, *Astrophys. J*, 431, 742
- [24] Zhuge, Xing, Centrella, J.M. and McMillan, S. L. W. 1994, *Phys. Rev.* D50, 6247
- [25] Zhuge, Xing, Centrella, J.M. and McMillan, S. L. W. 1996, *Phys. Rev.* D54, 7261
- [26] Oohara, K. and Nakamura, T. 1990, *Prog. Theor. Phys.* 83, 906
- [27] Nakamura, T. and Oohara, K. 1991, *Prog. Theor. Phys.* 86, 73
- [28] Shibata, M., Nakamura, T. and Oohara, K. 1992, *Prog. Theor. Phys.* 88, 1079-1095
- [29] Shibata, M., Nakamura, T. and Oohara, K. 1993, *Prog. Theor. Phys.* 89, 809-819

- [30] Ruffert, M., Janka, H. T. and Schaefer, G. 1996 *Astron. Astrophys.*311, 532-566
- [31] Ruffert, M., Janka, H. T., Takahasi, K. and Schaefer, G. 1997 *Astron. Astrophys.*319, 122-153
- [32] Oohara, K. and Nakamura, T. 1992, *Prog. Theor. Phys.*88,307
- [33] Ruffert, M., Rampp, M. and Janka, H. T. 1997 *Astron. Astrophys.*321, 991-1006
- [34] Kidder, L.E., Will, C. M. and Wiseman, A. G. 1992, *Class. Quantum Gravity*, 9, L125-31
- [35] Oohara, K., Nakamura, T. and Shibata, M. 1997, *Prog. Theor. Phys.*supplement 128, 183-250